LAWRENCE
LIVERMORE
NATIONAL
LABORATORY

UCRL-TR-229360

Melting of transition metals at high pressure and the influence of liquid frustration. I. The late metals Cu, Ni and Fe

M. Ross, R. Boehler, D. Errandonea

March 23, 2007

This work was performed under the auspices of the U.S. Department of Energy by University of California, Lawrence Livermore National Laboratory under Contract W-7405-Eng-48.

3-14-07

Melting of transition metals at high pressure and the influence of liquid frustration. I. The late metals Cu, Ni and Fe

Marvin Ross[1], Reinhard Boehler[2] and Daniel Errandonea[3]

[1]*Lawrence Livermore National Laboratory, University of California, Livermore, California 9455, USA*

[2]*Max Planck Institut für Chemie, Postfach 3060, D-55020 Mainz, Germany*

[3]*Departmento de Fisica Aplicada-ICMUV, Universitat de València, Edificio de Investigación, c/Dr. Moliner 50, 46100 Burjassot (Valencia), Spain*

This report focuses on the role that frustration, or preferred liquid local ordering, plays in the melting of transition metals. Specifically, Cu, Ni and Fe. It is proposed that for liquids of metals with partially filled *d*-bands (Ni and Fe) frustration caused by Peierls/Jahn-Teller distortion and pressure-induced *s-d* electron promotion provides a mechanism for creating and enhancing the stability of local structures. At the most elementary level, liquid structures are essentially impurities that lower the freezing point. In the case of transition metals with partially filled *d*-bands, the application of pressure induces *s-d* electron promotion increases the concentration of local structures. This leads to melting slopes for Ni and Fe that are considerably lower than measured for Cu, and lower than for theoretical predictions employing models in which liquid structures are neglected.

PACS numbers: 61.25. Mv, 64.70.DV, 64.70.Md, 62.50.+p

I. Introduction

The term *frustration*, as used in liquid physics, is defined as a geometric incompatibility between an energetically preferred local ordering, and an extended crystalline order tiling the entire space [1]. To date, discussions of liquid frustration have been largely confined to the glass transition. However, as we will attempt to show in the present report, frustration can have important consequences for the melting of metals. Melting measurements made for a number of transition metals at high pressure, have reported melting temperatures and melting slopes (dT/dP) that are surprisingly low[2-5], and defy the predictive capability of current theoretical techniques. In several earlier reports it had been proposed that the low melting slopes were due to the presence of local structures in the melt[6,7]. The idea, that local structures in liquid metals could be based on packing of five-fold symmetric icosahedral units was first suggested by Frank, in order to explain supercooling effects[8]. The icosahedron, has a lower energy/atom than bcc or fcc and hcp structures for clusters of up to several hundred atoms. Although it is impossible to create a crystal with icosahedral symmetry, randomly packed clusters with icosahedral short range order (ISRO) of varying sizes may evolve continuously and be interconnected throughout the liquid. Since icosahedral structures in a liquid maximize the local density, and are well matched to the five-fold symmetry of *d*-electron bonding, they are likely to influence transition metal melting.

Experimental evidence now exists confirming the presence of ISRO in several transition metal liquids [9-11]. They have been found in levitated liquid droplets of Ni, Fe, and Zr by Schenk et al.[9] using neutron scattering, and in Ni and Ti by Lee et al.[10] using *in situ* synchrotron x-ray diffraction. There is also experimental[11] and theoretical[12a,b] evidence for local structures in liquid and supercooled Ta, of a complex polytetrahedral nature with some icosahedral ordering. Density-functional-theory molecular-dynamic (DFT-MD) simulations made by Jaske et al. confirmed the presence of ISRO in Ni[13,14], Zr[15], and Ta melts[16].

Transition metals have strong directional bonding from incomplete *d*-bands and the formation of local structures in the liquid may be understood in terms of a Peierls/Jahn-Teller (P/JT) [17,18] distortion in which a system is stabilized by removing the degeneracy of levels, forming localized bonds, and lowering the energy. Figure 1 contains a summary of the measured high pressure melting slopes of several transitions metals, including Al[19], plotted versus the number of valence *d*-electrons calculated using electron band theory[20]. The plot shows that the lowest slopes occur for the early transition metals. The P/JT effect is optimal in the case of half-filled bands where the distortion lowers the energy of the occupied bonding states while the unoccupied anti-bonding states are raised in energy thus forming a narrow band gap. Lee et. al.[10] reported that the ISROs of early transition liquid metals are more distorted than those of late transition metal liquids possibly due to the greater angular dependence of *d*-bonding in the partially filled bands of the early metals. The close-packed metals Fe and Ni, which have a mix of bonding and anti-bonding electrons have higher melting slopes than the early transition metals. Cu and Al both lacking bonding *d*-electrons, have nearly the same relatively high melting slopes. Overall, these observations argue that the melting properties of transition metals are closely related to the P/JT effect and *d*-electron bonding.

All of the DAC melting data cited here [2-5] were obtained using the laser heated method, by observing the appearance in the liquid phase in a movement of the speckled laser light reflected pattern, by detecting a change in reflectivity [3], or by observing changes in the sample surface texture. Temperatures in the DAC experiments have been measured by spectroradiometry. In a separate set of experiments for Ta, and made at the Advanced Photo Source[4], the disappearance of crystalline x-ray diffraction lines[4] and the appearance of some diffuse broad scattering together with a substantial increase of the background provided a double check on the correctness of the original melting report[3]. These diagnostics have provided consistent melting data. Temperatures in all the experiments have been measured by spectro-radiometry.

Transition metals are particularly well suited as candidates for examining the influence of frustration on melting since, with few exceptions, they do not undergo solid-solid phase transitions along the melting curve that might complicate an understanding for the role of the liquid. In the present paper we examine the melting of several late transition metals for which there are high pressure melting measurements. In section II we examine the melting of Cu and Ni. Fe melting is in section III, and section IV is the Discussion. A subsequent paper (II) will examine melting of the early transition metals.

II. Melting of Cu and Ni

Cu and Ni are neighbors in the Periodic Table, with significant differences in the occupancy of the *d*-band that are useful for explaining the influence of the electronic structure on melting. Since Cu ($3d^{10}4s$) has a filled *d*-band lying below an *s*-like valence band at the Fermi surface, the *d*-band plays no role in chemical bonding. In contrast, Ni ($3d^{9}4s$) has an unfilled *d*-band at the Fermi energy and increasing the pressure increases the *d*-electron character due to *s*-*d* promotion[21,22]. Plotted in figure 2 are the melting measurements reported for Ni, by Lazor et al.[23], and by Japel et al.[5] for Cu and Ni. The Ni data for pressures above 60 GPa are the results of new measurements. The two sets of Ni DAC measurements, made at different laboratories, are in agreement.

The rather large difference in the Cu and Ni melting curves can be thought of as a consequence of "withdrawing" an electron from the filled Cu *d*-shell, to "create" Ni, which now has a partially filled *d*-shell which has the capacity to form locally preferred structures in the liquid[9,10]. In the case of Cu, x-ray absorption spectroscopy (XAS) studies lead to the conclusion that only weak icosahedral order could be observed[24,25]. This is consistent with the properties of isolated clusters, where Cu clusters are dominated by the delocalized outer *s*-electron forming closed shells similar to free atoms. In contrast, the properties of clusters with partially filled bands are determined by the localized behavior of *d*-electrons [26].

A. Free energy model

In order to illustrate the operative physics described above, but in a quantitative manner, we used a model that is based on the soft sphere inverse power equation of state. The model has been employed for Mo melting calculations where the derivation is treated in greater detail[6]. The thermodynamic properties for a system of atoms interacting by a repulsive inverse power potential $\phi(r)=C/r^n$ have been studied extensively by computer simulations [27,28]. A simplifying feature of this potential, is that it allows the excess Helmholtz free energy, and all of the thermodynamic

properties to be expressed as a function of a single parameter, the scaled inverse temperature;

$$\Gamma_n = \beta C/(a)^n. \qquad (5)$$

where $\beta=1/NkT$, a is the Wigner Seitz radius given by $4\pi n_o a^3/3=1$ and n_o is the atom number density. The excess Helmholtz free energy of the solid and liquid, can be expressed as,

$$F_{ex}^s = U_M + F_{th-invn}^s,$$
$$F_{ex}^l = U_M + F_{th-invn}^l.$$

The two terms in the solid and liquid excess free energy are, respectively, the Madelung energy(U_M) of the inverse power solid, and the ion-ion thermal free energies of the solid and liquid. Analytic expressions for the thermal free energy terms, for $n=1$ to 12, in terms of Γ are given elsewhere [27,28]. The ion-ion interaction was approximated by an inverse-ninth power potential.

A useful simplification[6], is to replace the Madelung energy, U_m, by U_{DAC} the energy determined from the analytic Birch-Murnaghan[29a] expression for the room temperature isotherm, and corrected to T=0 K. The excess Helmholtz free energy can now expressed written as,

$$F_{ex}^s = U_{DAC} + F_{th-inv9}^s. \qquad (6)$$
$$F_{ex}^l = U_{DAC} + F_{th-inv9}^l,$$

The model has the attractive feature that it reproduces the room temperature solid isotherm and employs a consistent set of solid and liquid free energy functions for the ion-ion potential determined from computer simulations. As a demonstration of its usefulness, the model is first applied to Cu. The B-M parameters for Cu, B_o= 135.1 GPa, and B_o'= 4.91 were obtained from room temperature DAC measurements [29b]. Melting calculations were made, by matching the Gibbs free energies of the two phases. It was determined that a value of C=800 eV-Å^9 fitted to the low pressure melting curve provided an excellent fit to higher pressure Cu melting measurements. These calculations are shown in figure 3. Also shown are the calculations of Belonoshko et al.[30] and Vocadlo et al.[31], that are also in agreement with the measurements. The

calculations by Belonoshko et al. were made by a solid-liquid phase coexistence molecular dynamics simulation, using an embedded-atom method(EAM) potential having five parameters fitted to energy and pressure data obtained from electron band calculations. Vocadlo et al. used the EAM potential of Belonoshko et al. as a reference to make coexistence simulations, then corrected the pressure and energy using ab-initio calculations.

B. Nickel melting

Plotted in figure 4, are the Ni DAC measurements[5], the computer simulations of Koci et al[32] and two sets of model calculations. The simulations of Koci et al. were made using the same computational method as Belonoshko et al.[30] made for Cu, except that the Ni EAM potential was fitted to low pressure experimental data. The reason for the failure of the computer simulation to agree with the Ni DAC measurements is that the EAM potential does not include the strong directional bonding arising from an incomplete *d*-electron valence band, and thereby lacks the capacity to form chemically preferred structures. In effect, by employing the EAM potential, Ni is treated as having a filled Cu-like *d*-band at all pressures, thereby behaving Cu-like.

In order to illustrate the physics, two sets of model calculations were made. In one set of calculations the presence of clusters are neglected, as in the Cu calculations(figure 2). In a second set clusters are introduced. The B-M parameters used for Ni, B_o= 184 GPa, and B_o'= 4.90, were obtained from a fit to the room temperature isotherm that had been obtained from a reduction of the Ni Hugoniot shock measurements[33]. The coupling parameter used here for Ni is C=800 eV-Å^9, the same value as used for Cu. For the melting curve omitting clusters this parameter provides a reasonable fit to the initial melting temperature, and is in good agreement with the EAM calculations of Koci et al. up to about 80 GPa.

While the structural re-orderings brought about by P/JT distortions are inevitable if the system is rigorously modeled, in the case of approximate models such those employing an EAM potential, or our free energy model, the influence of distortions needs to be introduced ad-hoc. Therefore, in the second set of model calculations, terms were added to the liquid free energy in order to account for the influence of clusters. The free energy of the liquid (eq. 6) is modified as,

$$F_{ex}^{l} = U_{DAC} + F_{th-inv9}^{l} + xU_{cl}^{l} + kT[x\ln x + (1-x)\ln(1-x)]. \qquad (7)$$

The added terms are the binding energy of a cluster, written as $U_{cl} = Eo(Vo/V)^{5/3}$, and the entropy of mixing, respectively. Vo is the initial volume. The variable x is the "generalized" cluster fraction. The value of *Eo* =-0.43 eV/atom employed here is the energy of a 13 atom closed icosahedron relative to a 13 atom fcc cluster, as calculated by Lathiotakis et al[34]. This approximation is based on the assumption that the energy of an icosahedron in a close-packed-like liquid scales approximately with the energy of a free icosahedron and a free fcc cluster. The volume dependence of the binding energy is assumed to be that of *d*-band electrons. The same value of the C potential coupling parameter was employed as in the previous calculation.

Typically, in thermodynamic models, the concentration fraction *x* can be determined by minimizing the free energy. However, in the present case, cluster formation and *s-d* electron promotion are quantum mechanical effects, and are not exclusively thermodynamically driven. The only alternatives to evaluate this parameter rigorously are extensive first principles calculations that are well beyond the scope of this report. Instead, and in the spirit of the modeling, *x* has been employed as a parameter used to fit the DAC measurements in order to extract the maximum amount of physical information needed to explain, rather than to predict, the experimental measurements.

While the calculated melting curve neglecting clusters is in agreement with the simulations, adding the cluster terms to the fluid phase lowers the melting temperature and the melting slope. The cluster fraction increases from x~0.0001 at low pressure to x~0.066 at 114 GPa, the highest pressure at which Ni melting was measured. At that pressure, the lowering of the liquid free energy due to clustering is about 5%, about half of which is the mixing entropy. It may be argued that the cluster binding energy *Eo* will be less than the assigned value. Nevertheless, the mixing entropy term will remain as a mechanism for lowering the liquid free energy and the melting temperature.

Although, EAM potentials are useful for their computational convenience, for the purpose of predicting melting curves, they are at best only justified for simple *sp*-bonded metals and series-end transition metals. The EAM potential does not include

strong directional *d*-electron bonding, or pressure induced *s-d* promotion, and as a consequence Ni is treated as Cu-like. Experimental evidence for the presence of local structures in the Ni melt[9,10], supports the inclusion of clusters in the free energy model, and provides the simplest explanation of the melting temperature measurements. The observed melting curve of Ni, and the low melting slope, is simply a classic example of freezing point lowering by a preferred structure acting as an impurity that is created and stabilized by pressure-induced *d*-electron promotion.

III. Iron Melting

An accurate knowledge of the Fe melting temperature at the Earth's inner-outer core boundary (IOCB) at 330 GPa is necessary in order to determine the planets thermal gradient and geodynamics. However, the response to this need has been complicated by, conflicting DAC and shock measurements, and theoretical predictions. These disagreements are apparent by the data in figure 5. Plotted here is the DAC melting curve of Fe measured up to 200 GPa [2]. Theoretical predictions made by Alfé et al.[35] and by Laio et al.[36]. And shock melting measurements of Brown and McQueen[37] and Nuygen and Holmes[38]. Also included in figure 5, for the purpose of comparison are the Cu and Ni DAC melting measurements reviewed in section II. In parts A and B below, an attempt is made to unravel the apparent disagreements between measurements and calculations.

A. DAC measurements and theoretical predictions

The Ni measurements shown in figure 5 follow the Fe measurements, and the Cu measurements follow the Fe calculations of Alfé et al. Based on our analysis of Cu and Ni melting in section 2, there is reason to suspect that the Fe calculations reported by Alfé et al. fail to correctly simulate the melt. Their calculations were made by employing the adiabatic switching method to calculate free energy[39,40]. The method starts with a system of atoms interacting by an inverse power potential and switches continuously to the system of interest, in this case iron, using *ab initio* density functional theory molecular dynamics (DFT-MD). At each step along the trajectory a full simulation is made for the coupled system and the ions are moved in accordance with the calculated forces. Since the free energy of the inverse-power system is well known, the free energy of the system of interest can be determined by adding to it the change in free energy calculated along the path. However, since the switching is an isentropic process it is inapplicable for calculating phase changes[40], and consequently local structure formation in the liquid is necessarily absent in the simulation. This would explain why

the predicted melting curve of Alfé et al. closely matches the Cu DAC measurements. While the switching method remains useful for carefully chosen systems like Cu, it is inapplicable for simulating Fe melting.

In the case of Laio et al.[36] a "force-matching" procedure was employed in which configurations in the solid and liquid are simulated by the DFT method and the pressure and energy is fitted to a parameterized local potential. The potential constructed in this way is not transferable to other P-T states, and the process needs to be repeated at many states along the melting curve. An overall effective potential is created and melting is calculated by a solid-liquid coexistence method. Unfortunately, the Letter published by Laio et al. is quite brief, and a more complete understanding of why their results agree with experiments is lacking.

B. Shock melting and evidence for local structures in the Fe melt at high pressure.

In shock experiments phase transitions are detected by discontinuities in the longitudinal sound speed. Brown and McQueen reported detecting two discontinuities in the sound velocity along the iron Hugoniot, at 200 GPa (~4000 K), and at 243 GPa (~5500 K). The first was identified as the onset of a solid-solid transition, and the second as the onset of shock melting. Temperatures quoted at shock pressures have to be calculated, since temperature measurements in experiments employing strong shocks are as yet unreliable. Recently, Nguyen and Holmes (NH) reported shock measurements, in which they detected only a single transition, that they interpreted as melting at 225 GPa (5100 ± 500 K). They did not find evidence for a solid-solid phase transition near 200 GPa. More recently, Brown[41] examined a definitive set of Los Alamos Hugoniot data[42], in the pressure range to 442 GPa and believes this data shows a small discontinuity in the density, of about -0.7%, at 200 GPa. Brown concludes, that a phase of iron other than hcp may be stable above 200 GPa.

A possible cause for the disagreement of DAC and shock melting measurements may be due to the presence of local structures in a viscous Fe melt. While direct evidence for ISRO in the iron melt at atmospheric pressure comes from the

measurements of Schenk et al.[9] and Lee et al.[10], evidence for increasing viscosity and the presence of local structures at elevated pressure comes from observations made in the DAC of the laser-speckle melt motion. For all materials ranging from noble gases[43], alkali halides [44], oxides[45] and metals [2-5] we observed that the vigor of motion of the laser-speckle at melting strongly decreased with increasing pressure along, and even far above the melting curve. Often, the disappearance of motion limited the pressure range of these melting measurements. The exact nature of the motion observed in the melt is not exactly clear, but apart from temperature gradients and the strength and surface tension of the pressure medium it is likely related to the viscosity of the melt. It should be pointed out that this observation is independent of the pressure medium used in these measurements. By comparing the vigor of motion (or fluidity) with that of common daily observations we can make a semi-quantitative estimate of the viscosities of the molten materials that is probably not less accurate than that of the numerous theoretical estimates.

At "low" pressures up to about 50 GPa we observe motions in liquid iron comparable to those observed in stirred light oil at ambient conditions (about 1 Pa s) and changes in the reflectivity that signify melting. The vigor of motion is certainly significantly lower than that measured for water or molten iron at one atmosphere (10^{-3} Pa s) or that observed for molten water at several tens of GPa [46] Above 70 GPa motion in liquid iron slows down significantly and appears comparable to that of wax or molten Hawaiian lava (10^{3}-10^{4} Pa s). An extrapolation of the visual estimates of the viscosity for liquid iron predicts a value of about 10^{6} Pa-s at the outer core boundary. At pressures of 100 GPa, and above, the speckle motion becomes undetectable and is no longer a useful diagnostic. It then becomes necessary to detect melting solely by observing changes in the reflectivity. The sudden loss of speckle motion implies the existence of a transition in the melt from a liquid to a highly viscous state near 100 GPa. Speckle motion is still not observed if temperatures are raised to exceed the melting temperatures by up to 1000 K suggesting pressure is the dominant effect on the viscosity. For a glass forming liquid just above the glass transition the viscosity is

typically of the order 10^{12} Pa-s. The estimated viscosities plotted in figure 6 are consistent with a picture in which the concentration of clusters of varying sizes increase with compression and finally jam near 100 GPa. A phase diagram of Fe, revised to include a liquid and very viscous phase of uncertain character is in figure 7. The relatively large increase in the melting slope above 100 GPa might be attributed to the fcc-hcp, but is more likely due to some limitation imposed on the pressure-induced entropy by the high viscosity.

Since molecular rearrangements are considered to scale roughly with viscosity[47], the absence of any speckle motion above 100 GPa, on the time scale of the DAC measurements, implies a relaxation rate in the viscous melt state near 200-250 GPa that is many orders of magnitude longer than the sub-microsecond time scales characteristic of shockwave generated phenomena. This suggests that the discrepancy in the melting pressure between the static and dynamic experiments is likely due to dynamic melting overshooting by about 25 GPa, or a density of only 1.9%[37]. An extrapolation of the Fe DAC measurements leads to a predicted melting temperature of ~5000 K near the IOCB at 330 GPa.

III. Discussion

In terms of elementary thermodynamics, locally preferred liquid structures in transition metal with partially filled *d*-bands act as impurities lowering the free energy and the melting temperature. With increasing pressure *s-d* promotion increases the concentration of local structures reducing the temperature rise and the melting slope. Similar physics appears to be present in systems with directionally bonded *p*-electrons[48]. In an earlier paper[6], it was proposed that the low melting temperatures and slopes found in the light actinide metals were also likely due to *f*-electron bonded local structures in the liquid. The light actinides, are distinct from the heavy actinides, in that their *f*-electrons participate in bonding in a manner similar to *d*-electrons in transition metals. However, in contrast to the highly symmetric structures formed by

the transition metals, the light actinide solids form low symmetry, open packed structures, that indicate a more covalent character of the chemical bond.

In a series of papers, Söderlind et al[49-51] have shown that a mechanism for understanding the stability of the *f*-electron bonding is a Peierls distortion of the crystal lattice which favors low symmetry. The P/JT mechanism is most effective if the energy bands are narrow, with a highly degenerate density of states near the Fermi surface. Using electron band theory calculations, Söderlind et al. showed that compared to the light actinides, the broader bands found in transition metals have less energy to gain from a Peierls distortion, as there are fewer energy levels at the Fermi surface. A survey of the available actinide melting curves[52] shows that light actinide metals have unusually low melting slopes. Whereas, transition metals, with broader bands less favored by P/JT distortions, typically have melting temperatures that are about 2 to 3 times higher than the actinides.

It is not fully accurate to imply that transition metals form only symmetric structures. The early transition metals, Sc, Ti and V, having a narrow *d*-band in a broad *sp*-band, form in stable cubic structures at ambient conditions. But with increasing pressure they undergo *sp-d* electron driven transfer to distorted structures[53-55]. This points out the fact that transition metal solids do have the potential to distort locally.

An unusual feature observed in the melting of xenon has been attributed to the presence of preferred structures[43]. Following a steep rise in temperature from 1 bar to 17 GPa(2750 K) there is a decrease in the melting slope(dT/dP) and a flattening of the melting temperature (dT/dP~0) near 3300K over the range 30 GPa to 80 GPa. The flattening of the melting slope has been attributed to pressure-induced *p-d* hybridization breaking the rare gas $5s^2p^6$ spherical symmetry, creating 5-fold symmetric icosahedral liquid structures, and thereby lowering the melting temperature from that predicted by a simple monatomic liquid. With a further increase of pressure to ~140 GPa the *5p-d* band gap closes and solid Xe becomes an early transition-like metal. The influence of preferred liquid structures on melting appears to be of broader consequence than is generally appreciated.

Acknowledgements: The work by MR was partially supported under the auspices of the U.S. Department of Energy by the University of California Lawrence Livermore National Laboratory under contract No. W-7405-ENG-48. D.E. acknowledges the financial support of the Spanish McyT through the RyC program. MR and D.E. also wish to thank the Max-Planck-Institute für Chemie at Mainz, Germany for its hospitality and the Alexander von Humboldt Foundation for its generous support.

References

1) G. Tarjus, S.A. Kivelson, Z. Nussinov and P. Viot, *J. Phy.:Condens. Matter* **17**, R1143 (2005): S.A. Kivelson, X. Zhao, D. Kivelson, T.M. Fischer and C.M. Knobler, *J.Chem.Phys.* **101**, 2391 (1994).

2) R. Boehler, *Nature (London)* **363**, 534 (1993).

3) D. Errandonea, B. Schwager, R. Ditz, C. Gessmann, R. Boehler and M. Ross, *Phys. Rev. B* ***63***, 132104 (2001).

4) D. Errandonea, M. Somayazulu, D. Häusermann and H.K. Mao, *J. Phy.:Condens. Matter* **15**, 7635 (2003); D. Errandonea, *Physica* B **357**, 356 (2005).

5) S. Japel, R. Boehler, B. Schwager and M. Ross, *Phys. Rev. Lett.* **95**, 167801 (2005).

6) M. Ross, L.H. Yang, and R. Boehler, *Phys. Rev. B,* **70**, 184112 (2004).

7) M. Ross, R. Boehler and S. Japel, *J. Phys. Chem. Solids*, 67, 2178 (2006).

8) F.C. Frank, *Proc. R. Soc. London*, Ser. A **215**, 43 (1952).

9**)** T. Schenk, D. Holland-Moritz, V. Simonet, R. Bellissent, and D.M. Herlach, *Phys. Rev. Lett.* **89**, 075507 (2002).

10**)** G.W. Lee, A.K. Gangopadhyay, K.F. Kelton, R.W. Hyers, T.J. Rathz, J.R. Rogers, and D.S. Robinson, *Phys. Rev. Lett.* **93**, 1982 (2004).

11) L. Cortella, B. Vinet. P.J. Desré, A. Pasturel, A.T. Paxton, and M. van Schilfgaarde, *Phys. Rev. Lett*. **70**, 1469 (1993).

12) C. Berne, A. Pasturel, M. Sluiter, and B. Vinet, *Phys. Rev. Lett.* **83**, 1621 (1999).

13) N. Jakse and A. Pasturel, *J.Chem.Phys.* **120**, 6124 (2004).

14) N. Jakse and A. Pasturel, *J.Chem.Phys.* **123**, 244512 (2004).

15 N. Jakse and A. Pasturel, *Phys. Rev. Lett.* **91**, 195501(2003).

16) N. Jakse, O. Le Bacq, and A. Pasturel, *Phys. Rev. B*. **70**,174203 (2004).

17) H.A. Jahn and E. Teller, *Proc. Soc. London, Ser.* A **161**, 220 (1937);

18) J.K. Burdett, *Chemical Bonding in Solids* (Oxford Univ. Press, Oxford, 1995).

19) R. Boehler and M. Ross, *Earth Planet. Sci. Lett.* **153**, 227 (1997).

20) H.L. Skriver, *Phys. Rev. B* **31**, 1909 (1985).

21) A.K. McMahan and R.C. Albers, *Phys. Rev. Lett*. **49**, 1198(1982).

22) A. K. McMahan, Physica **139**&**140**B, 31(1986).

23) P. Lazor, G. Shen and S.K. Saxena, *Phys. Chem. Minerals* 20, 86 (1993).

24) A. Di Cicco, A. Trapananti, S. Faggioni and A. Filipponi, *Phys. Rev. Lett.* **91**, 135505 (2003).

25) P. Ganesh, and M. Widom, *Phys. Rev.B*, **74**, 134205 (2006).

26) J.A. Alonso, *Chem. Rev*. **100**, 637 (2000).

27) H.E. DeWitt, "*Strongly Coupled Plasmas (1978)*", ed. G. Kalman and P. Carini (Plenum, New York, 1979) p.81.

28) D.H.E. Dubin and H. DeWitt, *Phys. Rev.* B **49**, 3043 (1994).

29a) E. Birch, J. Geophys. Res. **83**, 1257(1978).

29b) A. Dewaele, P. Loubeyre and M. Mezouar, *Phys. Rev.* B **70**, 094112 (2004).

30) A. B. Belonoshko, R. Ahuja, O. Eriksson and B. Johansson, *Phys. Rev.B*, **61**, 3838 (2000).

31) L. Vocadlo, D. Alfè, G.D. Price and M.J. Gillan, *J.Chem.Phys.***120**, 2872 (2004).

32) L. Kochi, et al., *Phys. Rev. B* **74**, 012101 (2006).

33) R.G. McQueen and S.P. Marsh, J. Appl. Phys. **31**, 1253(1960).

34) N.N. Lathiotakis, A.N. Andriotis, M. Menon and J. Connolly, J. Chem. Phys. **104**, 992(1996).

35) D. Alfé, L. Vocadlo, G.D. Price and M.J. Gillan, *J. Phys: Condens. Matter* **16**, S973-S982 (2004).

36) Laio et al., S. Bernard, G.L. Chiarotti, S. Scandolo and E. Tosatti, Science **287**, 1027 (2000).

37) J.M. Brown and R.G. McQueen, *J. Geophys. Res.* **91**, 7485 (1986).

38) J.H. Nuygen and N.C. Holmes, *Nature* **427**, 339 (2004).

39) M. de Koning, A. Antonelli, and S. Yip, *Phys. Rev. Lett.* **83**, 3973 (1999).

40) G. Grochola, *J.Chem. Phys.* **120**, 2122 (2004).

41) J. M. Brown, *Geoph. Res. Lett. **28***, 4339-4342 (2001).

42) R. S. Hixson, and J.N. Fritz, *J. Appl. Phys.* **71,** 1721(1992).

43) M. Ross, R. Boehler and P. Söderlind, *Phys. Rev. Lett.* **95**, 257801 (2005).

44) R. Boehler, M. Ross, D. B. Boercker, *Phys. Rev. Lett*. **78**, 004589 (1997).

45) A. Zerr and R. Boehler, *Nature* **371**, 506(1994); G. Serghiou, A. Zerr and R. Boehler, *Science* **280**, 2093(1998).

46) B. Schwager, L. Chudinovskikh, A.G. Gavriliuk and R. Boehler, *Phys.: Condens. Matter* 16, S1177-S1179 (2004).

47) D. Turnbull, *Contemp. Phys.* **10**, 473(1969).

48) V.V. Brazhkin, S.V. Popova and R.N. Voloshkin, *High Pressure Research* **15**, 267(1997).

49) P. Söderlind, O. Eriksson, B. Johansson, J.M. Wills and A.M. Boring, *Nature* **374**, 524(1995).

50) P. Söderlind, J.M. Wills and O. Eriksson, *Phys. Rev. B* **57**, 1320 (1998).

51) P. Söderlind, *Adv. Phys*. **47**, 9559 (1998).

52) D.A. Young, *Phase Diagrams of the Elements* (University of California Press, Berkeley, 1991).

53) Y. Akahama, H. Fujihisa and H. Kawamura, *Phys. Rev. Lett.* 94, 195503 (2005).

54) Y. Akahama, H. Kawamuraand T. Le Bihan, *Phys. Rev. Lett.* 87, 275503 (2001).

55) Y. Ding, R. Ahuja, J. Shu, P. Chow, W. Lei and H-k Mao, *Phys. Rev. Lett.* 94, 195503 (2007).

Figure captions

Fig. 1 High pressure melting slopes for several transition metals, including Al, plotted versus calculated number of valence *d*-electrons[20]. The dashed line is drawn as a guide to the eye.

Fig. 2 Cu and Ni melting curves. Experimental DAC Cu measurements by Japel et al.[5] Cu(open squares) and Ni(black circles), and by Lazor et al.[22] Ni(empty circles).

Fig. 3 Cu melting curves. DAC measurements(filled circles)[5] Calculations by Vocadlo et al.[31] (long dashes); simulations[30] and present free energy model.

Fig. 4 Ni melting curves. DAC Ni measurements for Ni (black circles)[5] and (empty circles)[22]. Computer simulated Ni melting(dashed curve)[32]. Free energy model calculations described in text made with(Model w) and without(Model wo) clusters.

Fig. 5 Fe, Ni, and Cu melting curves. DAC data for Fe[1](filled circles), for Ni (empty circles) and for Cu[5](green circles). Theoretical melting curves for Fe by Alfé et

al.[35](solid curve), and Laio et al.(dashed curve) [36]. Discontinuities in shock sound speed attributed to phase transition are those of BM(open squares)[37], and NH (filled squares)[38].

Fig. 6 Pressure dependence of the estimated iron melt viscosity at high hydrostatic pressure. The loss of speckle motion in the fluid is treated as a transformation to a glass.

Fig. 7. Phase diagram of Fe. Sold-melting(filled circles) and fcc-hcp boundary(empty circles and small dashed line)[2]. Vertical large dashed line, based on observations described in text, roughly defines a liquid to glass-like transition.

Figure 1

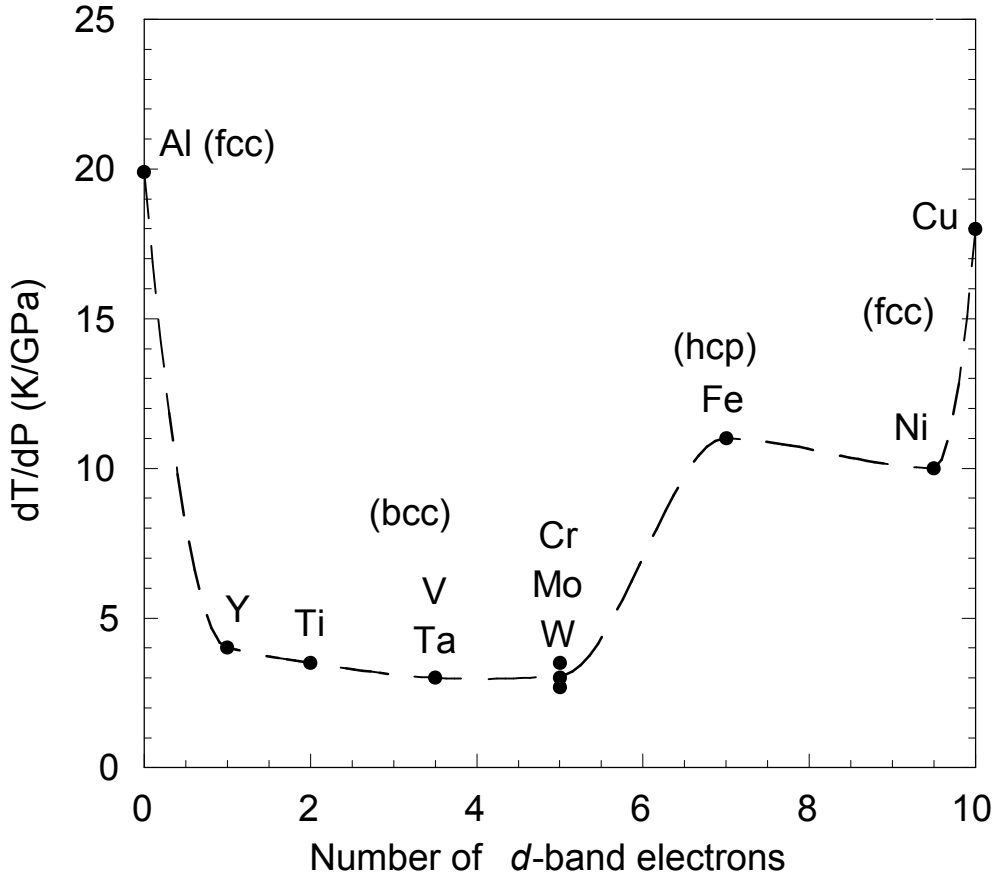
25
20
15
10
5
0
dT/dP (K/GPa)
Al (fcc)
Cu
(fcc)
(hcp)
Fe
Ni
(bcc)
Cr
Mo
W
V
Ta
Y
Ti
0
2
4
6
8
10
Number of d-band electrons

Figure 2

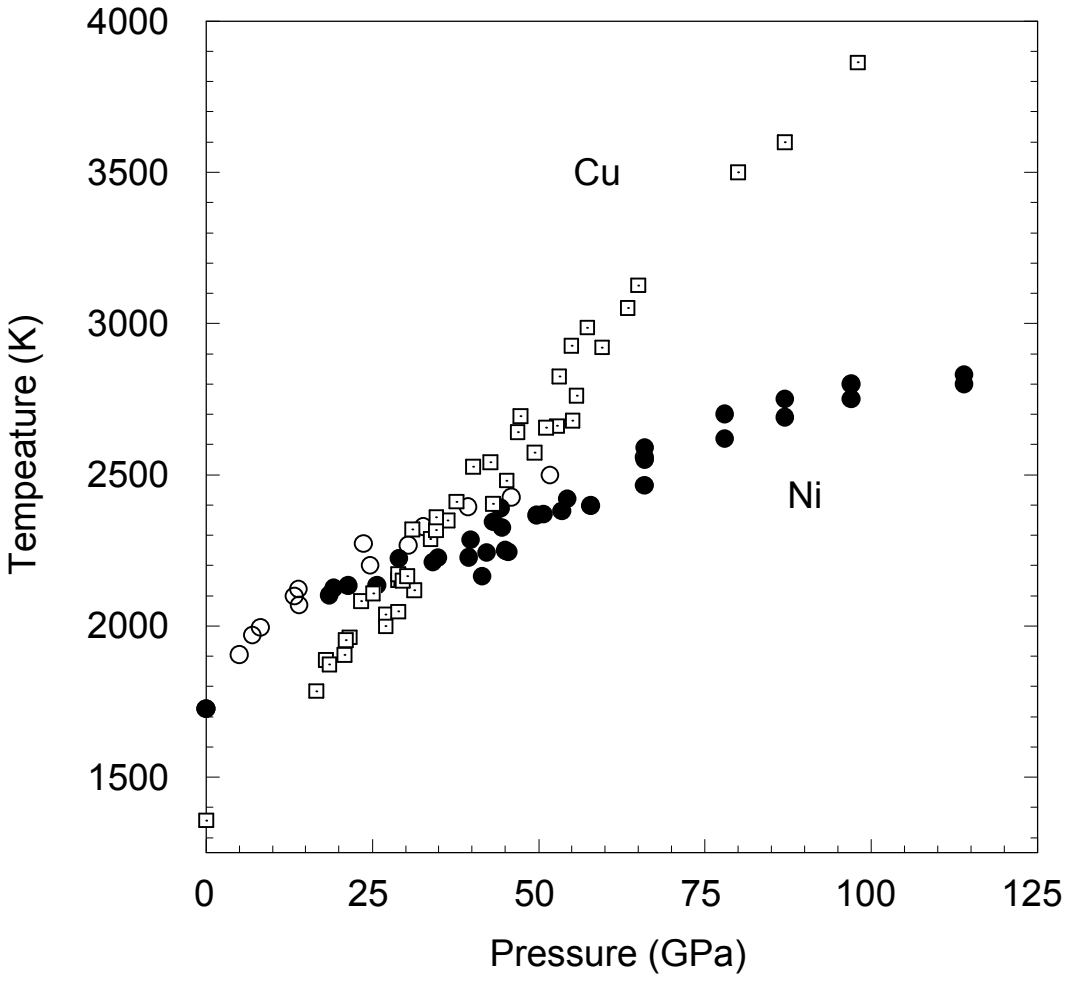
4000
3500
3000
2500
2000
1500
Tempeature (K)
Cu
Ni
0
25
50
75
100
125
Pressure (GPa)

Figure 3

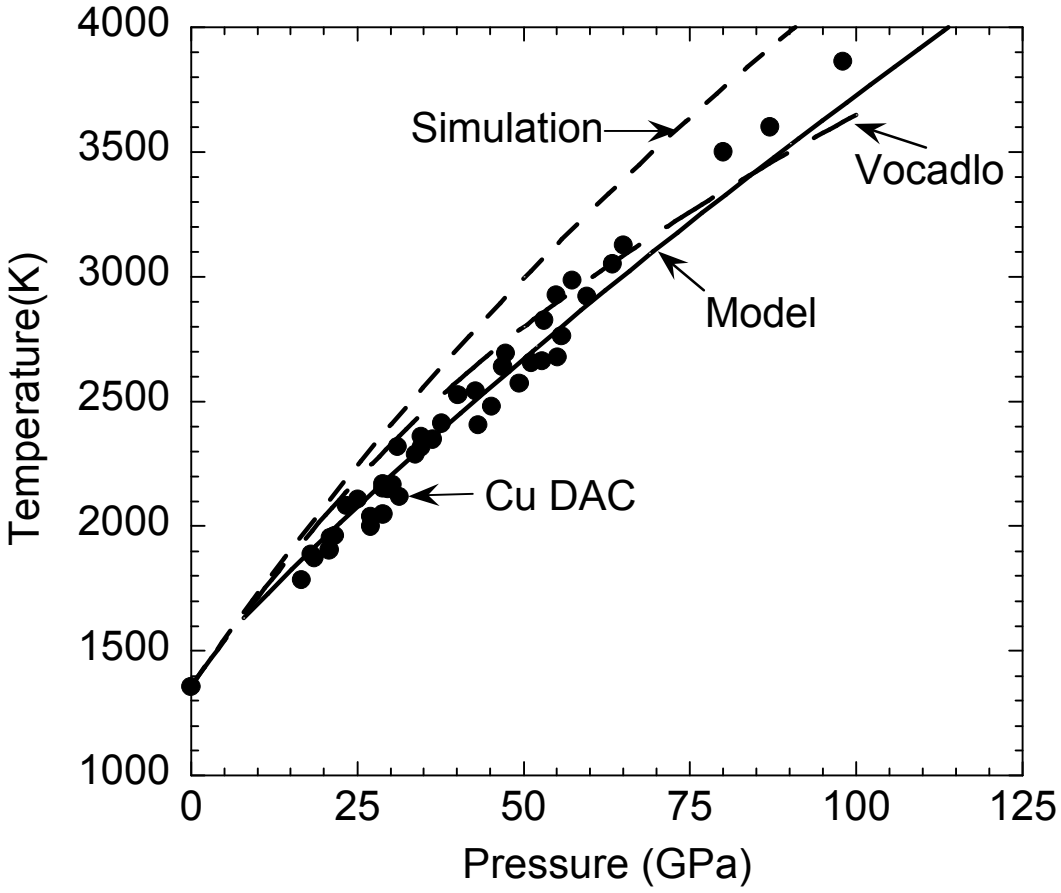
4000
3500
3000
2500
2000
1500
1000
Temperature(K)
0
25
50
75
100
125
Pressure (GPa)
Simulation
Vocadlo
Model
Cu DAC

Figure 4

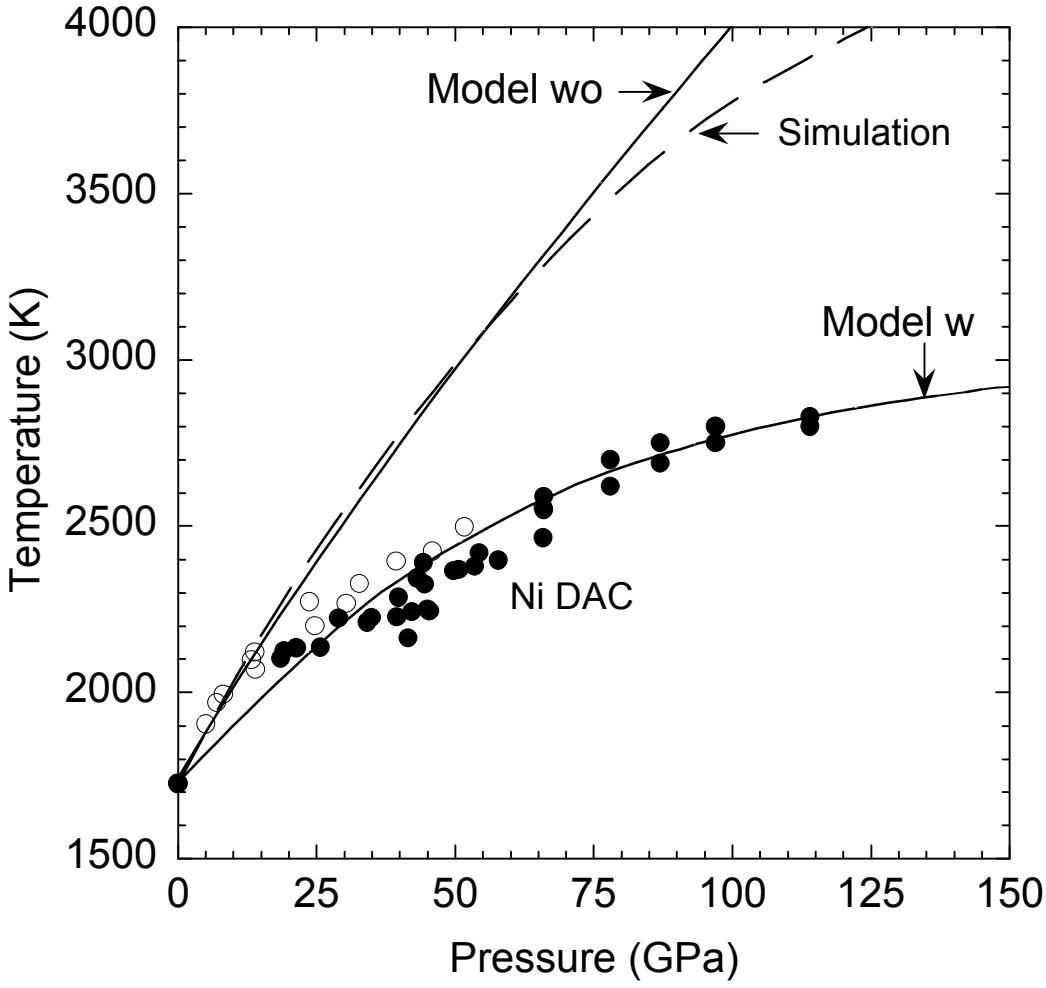
4000
3500
3000
2500
2000
1500
Temperature (K)
0
25
50
75
100
125
150
Pressure (GPa)
Model wo
Simulation
Model w
Ni DAC

Figure 5

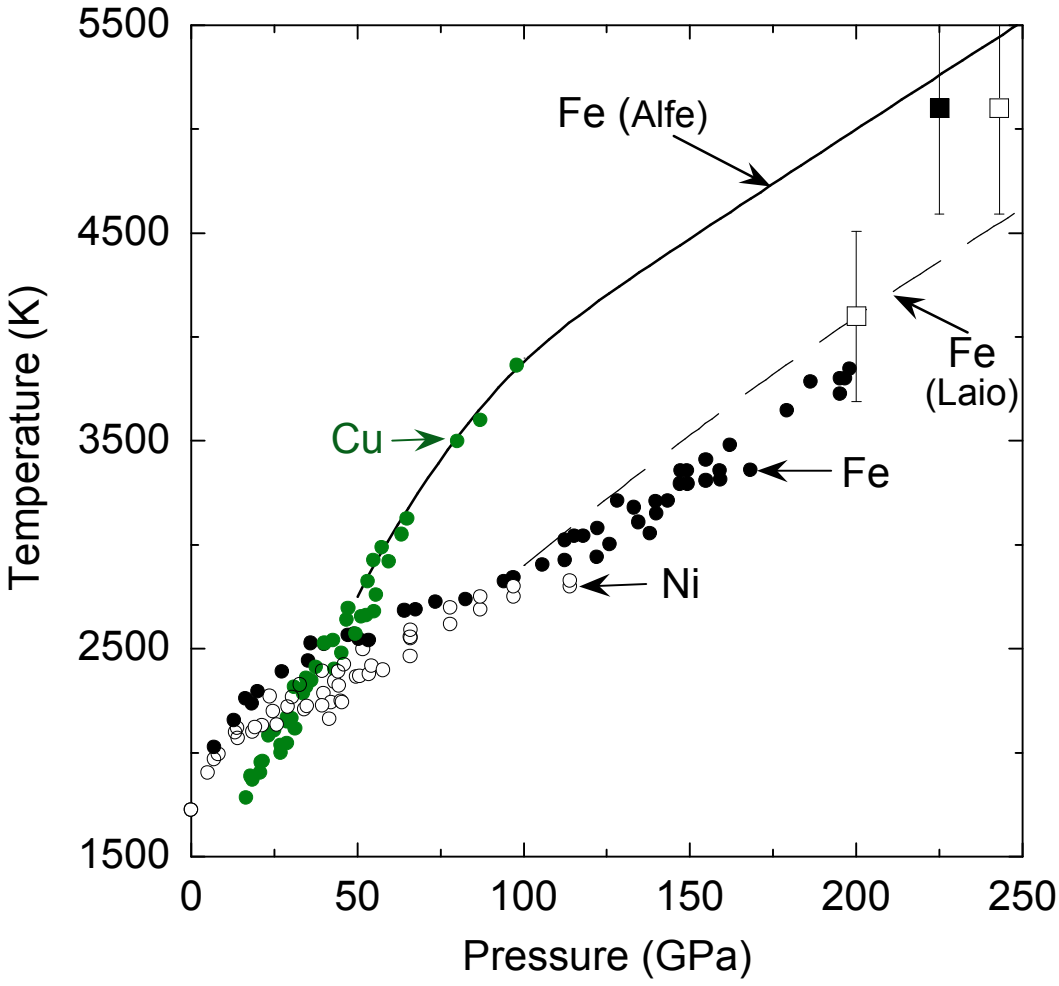
5500
4500
3500
2500
1500
Temperature (K)
0
50
100
150
200
250
Pressure (GPa)
Fe (Alfe)
Fe
(Laio)
Cu
Fe
Ni

Figure 6

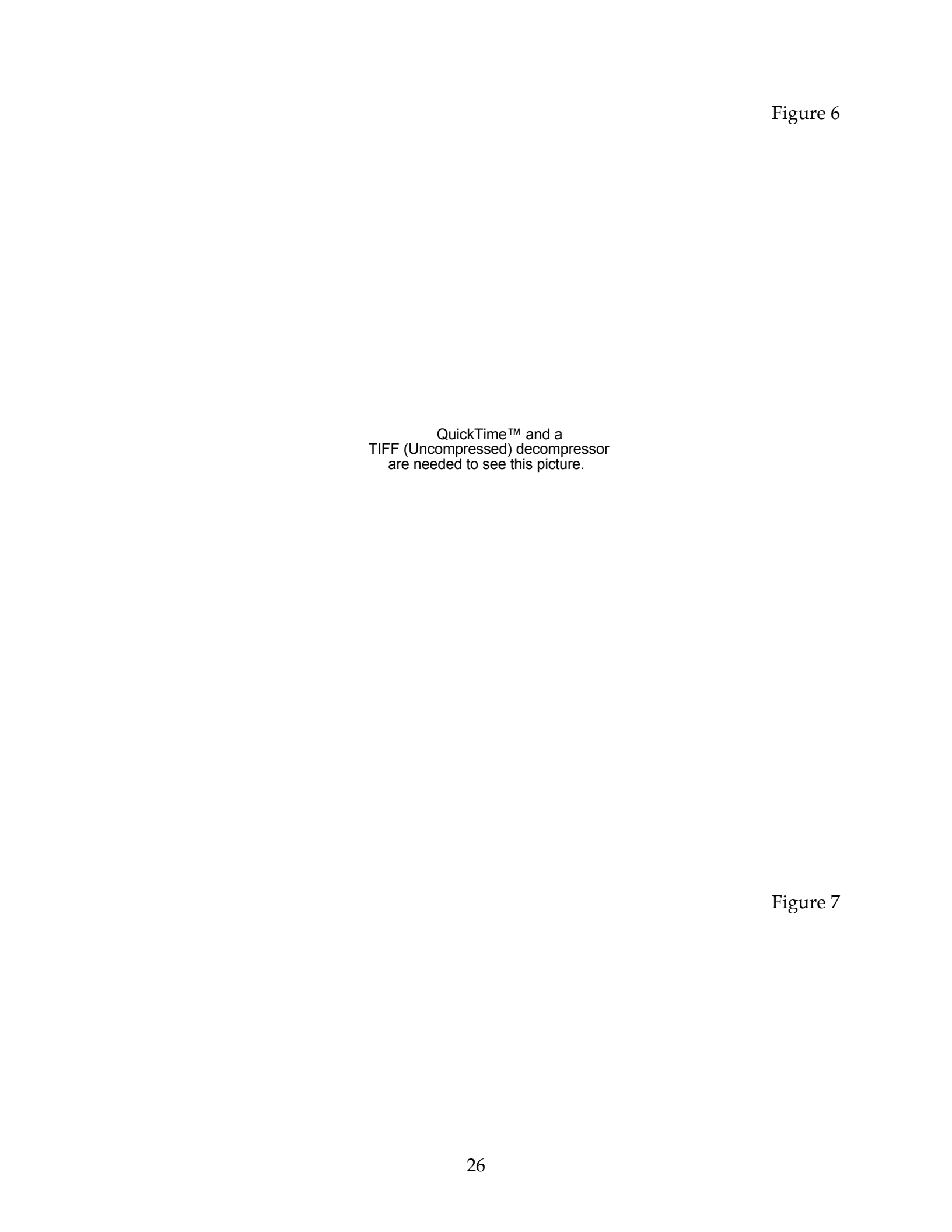

Figure 7

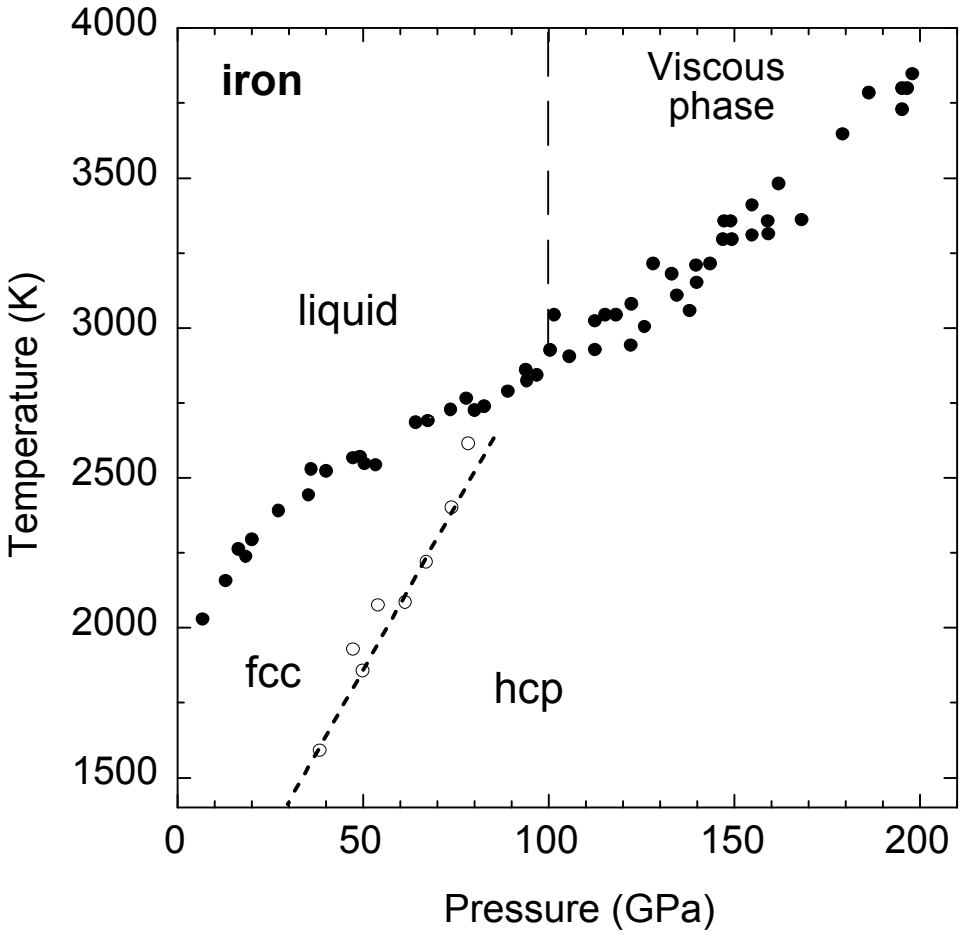
iron
Viscous
phase
liquid
fcc
hcp
Temperature (K)
Pressure (GPa)
4000
3500
3000
2500
2000
1500
0
50
100
150
200